SPARSE ADAPTIVE TEMPLATE MATCHING AND FILTERING FOR 2D SEISMIC IMAGES WITH DUAL-TREE WAVELETS AND PROXIMAL METHODS

Mai Quyen Pham[1,3], *Caroline Chaux*[2], *Laurent Duval*[1], *and Jean-Christophe Pesquet*[3]

[1] IFP Energies nouvelles
Control, Signal and System Department
1 et 4 avenue de Bois-Préau
92852 Rueil-Malmaison, France
laurent.duval@ifpen.fr

[2]Aix-Marseille Université, CNRS,
Centrale Marseille, I2M, UMR 7373,
39 rue F. Joliot-Curie,
13453 Marseille, France
caroline.chaux@univ-amu.fr

[3]Université Paris-Est
LIGM UMR-CNRS 8049
5 bd Descartes,
77454 Marne-la-Vallée, France
{Mai-Quyen.pham, pesquet}@univ-mlv.fr

ABSTRACT

This paper proposes a novel approach for echo-like multiple removal in two-dimensional seismic images. It is based on constrained adaptive filtering associated with geometric wavelets. Approximate templates of multiple reflections are assumed to be available and they are matched to multiple reflections throughout estimated finite impulse response filters. The problem is formulated under a constrained convex optimization form where the data of interest and filters are estimated jointly. Proximal approaches are used to perform the minimization of the derived criterion. The effectiveness of the proposed approach is demonstrated with various noise levels on realistic simulated data and on field seismic data.

Index Terms— Convex optimization, Parallel algorithms, Wavelets, Adaptive filters, Geophysics, Sparsity.

1. INTRODUCTION

In reflection seismology, a seismic source is generated at the ground surface or underwater. The resulting seismic wave front travels through the earth and is reflected at geological interfaces where changes in propagating medium density and velocity occur. The energy reflected back to the surface is recorded for geophysical processing, to provide estimates of subsurface structures. One distinguishes two main types of reflections: 1) primaries, reflected upward only once and 2) multiples, similar to acoustic reflections bouncing several times. Reflections, related to geology, take the shape of specific patterns [1] in seismic images, as illustrated in Fig. 1. We address the problem of template matching [2] and sparse adaptive multiple reflection filtering. It consists in finding parts in the seismic image that approximately match pre-defined templates, and in adaptively subtracting them (Fig. 1-middle) from the seismic data (Fig. 1-left) to uncover precious obfuscated geological information (Fig. 1-right). This concept is akin to disocclusion, visual echo cancellation [3] or template matching [2, 4] in pattern recognition. The main difference lies in the lack of rotation or scale degrees of freedom in the templates. In contrary to traditional objects, seismic waves have a non-bounded support, and exhibit a band-limited spectral content, closer to fingerprints or geometric textures [5]. Meanwhile, seismic templates are obtained through geophysical modelling. They are only approximate, and substantially differ from the geophysical reality in nonstationary amplitude, time delay and frequency content. They ought to be matched to multiple reflections through adapted finite impulse response (FIR) filters that are estimated jointly with the signal of interest (primary).

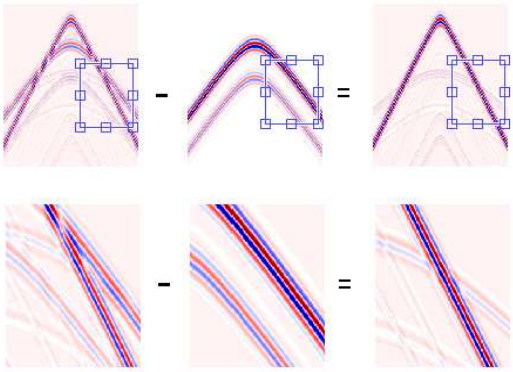

Fig. 1. Left to right: observed image z, multiple $\overline{s}$, primary $\overline{y}$.

Traditionally, adaptive multiple removal is performed in two or three dimensional seismic data, via standard ℓ_2- or more robust ℓ_1-norms, with local multidimensional matching FIR filters. The multidimensionality of the filters is thought to ensure lateral continuity in seismic events. A quite opposite direction was taken in [6], with an emphasis on a frequency- and shift-insensitive complex wavelet transform frame, associated with simple unary (one-tap) complex filters, in 1D only. Counter-intuitively, it was able to perform similarly to more classical 2D matching techniques. In other words, a careful partnership between sparse representations and adaptive filtering was deemed beneficial in 1D, with respect to traditional 2D methods. To account for additional properties, including statistical distributions for primaries [7] and slow filter variations, [8, 9] pursued seismic data adaptive filtering with 1D wavelet frames. Meanwhile, seismic images possess geometric regularity that advises a 2D approach for improved per-

$$\begin{bmatrix} R_j^{(0,n_x)} \\ \vdots \\ R_j^{(N_t-1,n_x)} \end{bmatrix} = \begin{bmatrix} r_j^{(-p',n_x)} & \dots & r_j^{(0,n_x)} & 0 & \dots & 0 \\ r_j^{(-p'+1,n_x)} & \dots & & r_j^{(0,n_x)} & 0 \dots & 0 \\ \vdots & & & & & \\ r_j^{(N_t-1,n_x)} & r_j^{(N_t-2,n_x)} & & \dots & & r_j^{(N_t-P_j,n_x)} \\ 0 & r_j^{(N_t-1,n_x)} & & \dots & & r_j^{(N_t-P_j+1,n_x)} \\ \vdots & & & & & \\ 0 & \dots & 0 & r_j^{(N_t-1,n_x)} & \dots & r_j^{(N_t-P_j-p',n_x)} \end{bmatrix}. \quad (1)$$

formance. As a result, multiscale geometric transforms such as curvelet frames [10–12] have been employed in geophysical processing. Indeed, 2D matching filters resemble directional filters [13]. We extend here [8] to 2D seismic data. Its anisotropy arises from seismic wave propagation and the nature of array acquisition. One dimension of seismic images is governed by space (sensor location) while the other dimension reflects time (wave propagation). This is directly modelled in the proposed scheme. We adopt a variational framework and build a criterion to be minimized where 1) a data fidelity term fits the seismic image formation model, and 2) regularization terms (constructed as hard constraints) express a priori information one expects on adapted FIR filters and the primary. The derived convex minimization problem is solved using iterative proximal algorithms. The remainder of the paper is organized as follows: Section 2 presents the model and the proposed method. Simulation results are evaluated both subjectively and objectively in synthetic data and visually of field seismic data in Section 3. Section 4 concludes the paper.

2. MODELLING MULTIPLE REFLECTIONS

A line of seismic sensors delivers a two-dimensional image. Each column is formed by a 1D temporal signal acquired by one sensor:

$$z^{(\mathbf{n})} = \overline{s}^{(\mathbf{n})} + \overline{y}^{(\mathbf{n})} + b^{(\mathbf{n})} \quad (2)$$

with $\mathbf{n} = (n_t, n_x)$, where $n_t \in \mathcal{N}_t \triangleq \{0, \dots, N_t - 1\}$ is the time index, $n_x \in \mathcal{N}_x \triangleq \{0, \dots, N_x - 1\}$ is the sensor index, and $\mathbf{n} \in \boldsymbol{\mathcal{N}} \triangleq \{(n_t, n_x) | \, n_t \in \mathcal{N}_t, \, n_x \in \mathcal{N}_x\}$. Observed data $z = (z^{(\mathbf{n})})_{\mathbf{n}\in\boldsymbol{\mathcal{N}}}$ (Fig. 1-left) is composed of the primary $\overline{y} = (\overline{y}^{(\mathbf{n})})_{\mathbf{n}\in\boldsymbol{\mathcal{N}}}$ (Fig. 1-right, 2D data of interest, unknown), multiples $(\overline{s}^{(\mathbf{n})})_{\mathbf{n}\in\boldsymbol{\mathcal{N}}}$ (sum of undesired reflected data, in Fig. 1-middle) and additive noise $(b^{(\mathbf{n})})_{\mathbf{n}\in\boldsymbol{\mathcal{N}}}$. One assumes that genuine multiples $(\overline{s}^{(\mathbf{n})})_{\mathbf{n}\in\boldsymbol{\mathcal{N}}}$ can be estimated as a local, weighted sum of template candidates:

$$\overline{s}^{(\mathbf{n})} = \sum_{j=0}^{J-1} \sum_{p=p'}^{p'+P_j-1} \overline{h}_j^{(\mathbf{n})}(p) r_j^{(n_t-p,n_x)} \quad (3)$$

Here $(r_j^{(\mathbf{n})})_{\mathbf{n}\in\boldsymbol{\mathcal{N}},0\leq j<J}$ denote J available templates and $\overline{h}_j^{(\mathbf{n})}$ is the unknown impulse response (with P_j coefficients) for template r_j at time n_t and sensor n_x (the filtering process is both time and space variant) and where $p' \in \{-P_j+1, \dots, 0\}$ ($p' = 0$ corresponds to the causal case). Eq. (3) can be expressed more concisely as

$$\overline{s} = \sum_{j=0}^{J-1} R_j \overline{h}_j \quad (4)$$

where

$$\overline{s} = \Big[\overline{s}^{(0,0)}, \dots, \overline{s}^{(N_t-1,0)}, \dots, \overline{s}^{(0,N_x-1)}, \dots, \overline{s}^{(N_t-1,N_x-1)}\Big]^\top,$$

$$\overline{h}_j = \Big[\overline{h}_j^{(0)\top}, \dots, \overline{h}_j^{(N_x-1)\top}\Big]^\top$$

and

$$\overline{h}_j^{(n_x)} = \Big[\overline{h}_j^{(0,n_x)}(p'), \dots, \overline{h}_j^{(0,n_x)}(p'+P_j-1), \dots, \overline{h}_j^{(N_t-1,n_x)}(p'), \dots, \overline{h}_j^{(N_t-1,n_x)}(p'+P_j-1)\Big]^\top.$$

The matrix R_j is block diagonal. Its diagonal elements are denoted by $(R_j^{(n_t,n_x)})_{n_t\in\mathcal{N}_t}$ and are given in (1). By defining $\mathbf{R} = [R_0 \cdots R_{J-1}] \in \mathbb{R}^{N_tN_x \times N_tN_xP}$ and $\overline{\mathbf{h}} = [\overline{h}_0^\top \cdots \overline{h}_{J-1}^\top]^\top \in \mathbb{R}^{N_tN_xP}$, with $P = \sum_{j=0}^{J-1} P_j$, Model (2) can be rewritten more concisely as

$$z = \mathbf{R}\overline{\mathbf{h}} + \overline{y} + b. \quad (5)$$

We propose a variational framework where we aim at estimating simultaneously the filter tap coefficients of the nonstationary filter $\overline{\mathbf{h}}$ and the primary $\overline{y}$. The multiple removal problem is thus formulated as the following constrained convex minimization problem

$$\underset{y\in\mathbb{R}^{N_tN_x},\, \mathbf{h}\in\mathbb{R}^{N_tN_xP}}{\text{minimize}} \; \|z - y - \mathbf{R}\mathbf{h}\|_2^2 + \iota_D(Fy) + \iota_C(\mathbf{h}), \quad (6)$$

where $F \in \mathbb{R}^{KN_x \times N_tN_x}$ models a frame operator (e.g. directional wavelets [15]). Functions ι_C and ι_D denote indicator functions of nonempty convex sets C and D, respectively i.e. $\iota_C(x) = 0$ if $x \in C$ and $\iota_C(x) = +\infty$ if $x \notin C$. Generally, seismic data exhibits geometric features (linear, hyperbolic

and parabolic), at least piecewise, corresponding to subsurface interfaces (Fig. 1). Due to the anisotropic nature of seismic data, we choose F as a hybrid dual-tree wavelet (with different wavelets along space and time [16]). Their decorrelation properties [17] have proven efficient in textured image denoising [18, 19], compared to curvelets whose redundancy is more important. We now turn our attention to the choice of the convex sets C and D.

2.1. Definition of convex set D

The relation $x = Fy$ relates the primary data y to the transform coefficients, denoted by x. They exhibit specific subband structures that are exploited here. Therefore, the constraint can be split by defining a partition of $\{1, \dots, KN_x\}$ denoted by $\{\mathbb{K}_l \cup \mathbb{K}_{l+\mathcal{L}} \mid l \in \{1, \dots, \mathcal{L}\}\}$, where $\mathcal{L}$ corresponds to the number of subbands, $\mathbb{K}_l$ and $\mathbb{K}_{l+\mathcal{L}}$ are the l-th subband corresponding to the primal and dual coefficients, respectively. Then, one can choose $D = D_1 \times \cdots \times D_{\mathcal{L}}$ where, for every $l \in \{1, \dots, \mathcal{L}\}$, $D_l = \{(x_k)_{k\in\mathbb{K}_l\cup\mathbb{K}_{l+\mathcal{L}}} \mid \sum_{k\in\mathbb{K}_l} \varphi_l(x_k) \leq \beta_l \text{ and } \sum_{k\in\mathbb{K}_{l+\mathcal{L}}} \varphi_l(x_k) \leq \beta_l\}$, $\varphi_l : \mathbb{R} \to [0, +\infty[$ is a lower-semicontinuous convex function. One natural choice for φ_l is the ℓ_1-norm.

2.2. Definition of convex set C

The convex set C introduces a priori knowledge on filter tap coefficients. As mentioned earlier, filters are assumed to vary along the time n_t and the sensor index n_x. However, their variations are usually slow. This can be modelled by the following two constraint convex sets C_1 (variations along time) and C_2 (variations along the sensors):

$$\begin{aligned} C_1 =& \Big\{ h \in \mathbb{R}^{N_t N_x P} \mid \forall (j, n_t, n_x, p), \\ & \qquad |h_j^{(n_t+1, n_x)}(p) - h_j^{(n_t, n_x)}(p)| \leq \varepsilon_{j,p}^{n_x} \Big\} \\ C_2 =& \Big\{ h \in \mathbb{R}^{N_t N_x P} \mid \forall (j, n_t, n_x, p), \\ & \qquad |h_j^{(n_t, n_x+1)}(p) - h_j^{(n_t, n_x)}(p)| \leq \varepsilon_{j,p}^{n_t} \Big\}, \end{aligned} \tag{7}$$

where $(\varepsilon_{j,p}^{n_x}, \varepsilon_{j,p}^{n_t}) \in [0, +\infty[^2$. Moreover, additional a priori information can be added directly on the vector of filter coefficients $\mathbf{h}$. This amounts to defining a new convex set C_3 as a lower level set of some proper lower-semicontinuous convex function ρ, by setting $C_3 = \big\{\mathbf{h} \in \mathbb{R}^{N_t N_x P} \mid \rho(\mathbf{R}\mathbf{h}) \leq \lambda\big\}$, where $\lambda \in \,]0, +\infty[$ and $\rho \colon \mathbb{R}^{N_t N_x} \to [0, +\infty[$ is a lower-semicontinuous convex function. Finally, C can be expressed as $C = C_1 \cap C_2 \cap C_3$.

To minimize the resulting sum of convex functions composed with linear operators, we choose to employ a primal-dual algorithm [20] an example of which is the Monotone+Lipschitz Forward-Backward-Forward (M+L FBF) algorithm [21]. Initially, the M+L FBF requires to compute proximity operators [22] for which closed form expressions exist for numerous functions [23]. However, they reduce here to computing projections onto D and $(C_\tau)_{\tau\in\{1,2,3\}}$ as the functions to be minimized correspond to indicator functions of nonempty convex sets D and $(C_\tau)_{\tau\in\{1,2,3\}}$ respectively.

3. SIMULATIONS

Our method is evaluated on the 2D synthetic seismic dataset presented in Fig. 1 with $N_x = 512$ seismic traces of length $N_t = 512$. The primary and two templates are obtained from suitably filtered real seismic data as in [8], plugged into (3) with filters of length $P_0 = 4$ and $P_1 = 5$.

The constraint sets C_1 and C_2 are defined by (7) where, for every (j, p, n_t, n_x), $\varepsilon_{j,p}^{n_x} = 0.05$ and $\varepsilon_{j,p}^{n_t} = 0.0001$. Regarding convex sets D and C_3, we choose $\varphi_l = |\cdot|$, and we investigate three possible choices for ρ, for every $d \in \mathbb{R}^{N_t \times N_x}$:

1. ℓ_1-norm: $\ell_1(d) = \sum_{n_x=0}^{N_x-1} \sum_{n_t=0}^{N_t-1} |d^{(n_t,n_x)}|$,
2. ℓ_2-norm: $\ell_2(d) = \sqrt{\sum_{n_x=0}^{N_x-1} \sum_{n_t=0}^{N_t-1} (d^{(n_t,n_x)})^2}$,
3. $\ell_{1,2}$-norm: $\ell_{1,2}(d) = \sum_{n_x=0}^{N_x-1} \left(\sum_{n_t=0}^{N_t-1} (d^{(n_t,n_x)})^2 \right)^{1/2}$.

		σ	0.04	0.08	0.16
Observation error		$\ell_1(\times 10^2)$	3.88	6.89	13.1
		$\ell_2(\times 10^2)$	5.42	8.80	16.4
1D version [8]		$\ell_1(\times 10^2)$	2.05	2.91	4.07
		$\ell_2(\times 10^2)$	4.75	6.26	8.06
ℓ_1	orthogonal basis$^{(*)}$	$\ell_1(\times 10^2)$	1.66	2.33	3.37
		$\ell_2(\times 10^2)$	2.96	3.78	5.40
	SI frame$^{(*)}$	$\ell_1(\times 10^2)$	1.23	1.70	2.39
		$\ell_2(\times 10^2)$	2.51	2.93	3.86
	M-band dual-tree$^{(*)}$	$\ell_1(\times 10^2)$	**1.14**	**1.47**	**2.00**
		$\ell_2(\times 10^2)$	**2.42**	**2.66**	**3.30**
ℓ_2	orthogonal basis$^{(*)}$	$\ell_1(\times 10^2)$	1.53	2.27	3.34
		$\ell_2(\times 10^2)$	2.56	3.59	5.33
	SI frame$^{(*)}$	$\ell_1(\times 10^2)$	1.19	1.69	2.42
		$\ell_2(\times 10^2)$	2.34	2.93	4.01
	M-band dual-tree$^{(*)}$	$\ell_1(\times 10^2)$	**1.07**	**1.41**	**1.96**
		$\ell_2(\times 10^2)$	**2.20**	**2.50**	**3.20**
$\ell_{1,2}$	orthogonal basis$^{(*)}$	$\ell_1(\times 10^2)$	1.51	2.25	3.32
		$\ell_2(\times 10^2)$	2.48	3.54	5.27
	SI frame$^{(*)}$	$\ell_1(\times 10^2)$	1.10	1.58	2.32
		$\ell_2(\times 10^2)$	1.76	2.36	3.49
	M-band dual-tree$^{(*)}$	$\ell_1(\times 10^2)$	**0.95**	**1.31**	**1.87**
		$\ell_2(\times 10^2)$	**1.60**	**2.07**	**2.83**

Table 1. Comparison of the results obtained by the proposed 2D dual-tree wavelets with the 1D [8] and different 2D$^{(*)}$ wavelet transforms, over three noise levels, and three a priori functions $\rho \in \{\ell_1, \ell_2, \ \ell_{1,2}\}$.

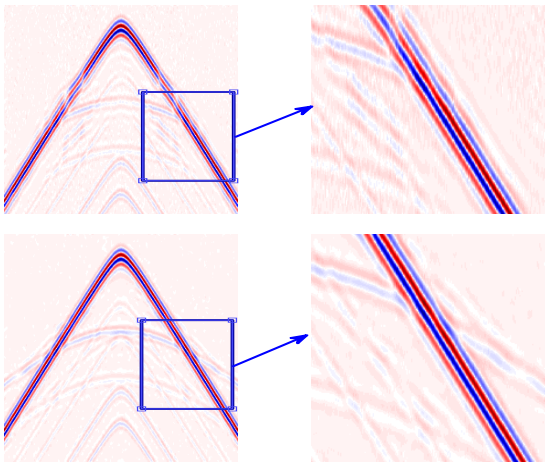

Fig. 2. Estimated y by 1D method [8] (top) and by 2D method (bottom) from observed data z (with $\sigma = 0.04$ in Figure 1).

We compute projections onto the convex sets C and D similarly as in [8]. The transforms are chosen as follows. In the time (vertical or sensor) and in the space directions, we choose a Symmlet of length 8 and a Daubechies wavelet of length 4, respectively. The overall transform F may either be: 1D shift-invariant (SI, length-8 Symlet along time only), 2D critical and orthogonal, 2D shift-invariant (fully redundant) or 2D dual-tree (twice redundant). In the latter case, the given wavelets yield the primal tree, the dual being obtained by the Hilbert transform of the aforementioned wavelets. The constraint bounds $\big((\beta_l)_{l\in\{1,\dots,L\}}$ and $\lambda\big)$ are computed empirically on i) real signals for synthetic data and ii) estimated signals using [6] for real data.

In Fig. 2, the top row shows the SI-1D wavelet frame result, although more redundant tight-frame are used, exhibits a higher level of remnant noise and a blur crossing, as opposed to the bottom row, where primaries are clearly recovered with the proposed 2D version using the dual-tree wavelet. The comparison is pursued in a more complete and objective manner with ℓ_1 and ℓ_2 residual errors for primaries $\overline{y} - \hat{y}$ in Tab. 1 in which the values in bold indicate the minimum residual errors for each ρ. We test the proposed method against different levels of noise: $\sigma \in \{0.04, 0.08, 0.16\}$ and three different ρ functions. We see that 2D versions generally further reduce modelling errors, as expected. Moreover, a loose ranking is as follows: SI-1D $<$ Ortho-2D $<$ SI-2D $<$ dual-tree, and the smallest absolute or quadratic residuals are obtained with the $\ell_{1,2}$-norm. This confirms that mild redundancy and directionality in the sparsifying transform are indeed beneficial over (potentially more redundant) 1D and separable 2D decompositions, when coupled with appropriate constraints.

Fig. 3 displays a recorded seismic data with a partially appearing primary (arrows) and the estimated primaries obtained by 1D version [8] and by 2D version. We refer to [6] for template construction. The outcome is displayed in the cropped square zone from recorded seismic data only. The primary is better delineated with the directional dual-tree wavelet frame, with a reduced level of remaining noise and multiple interferences. Additional results are given in [24].

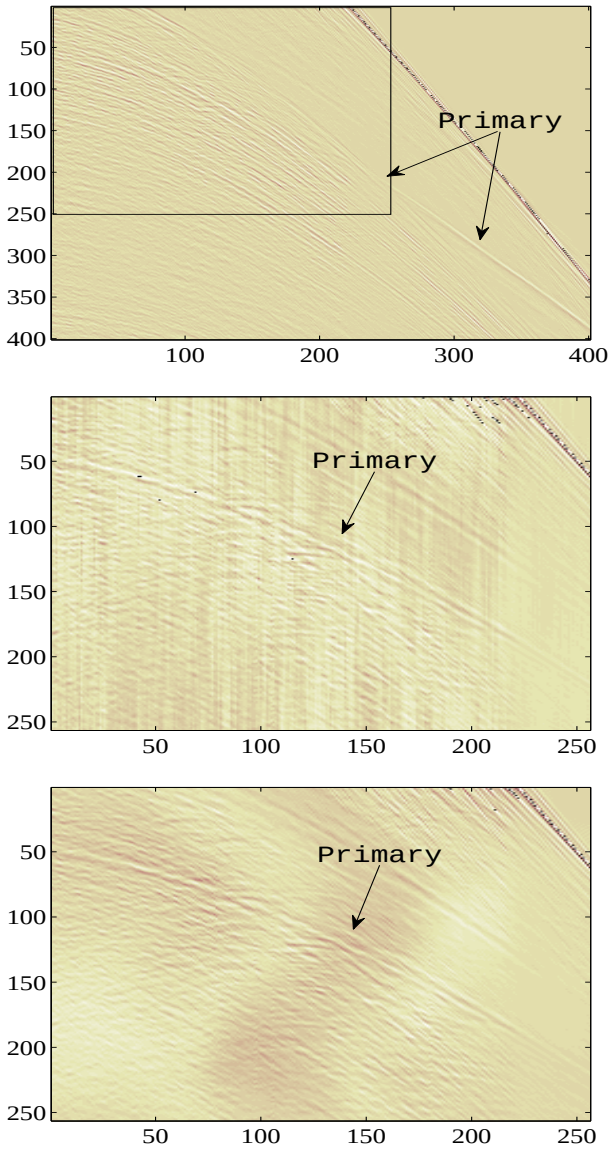

Fig. 3. From top to bottom: recorded seismic data with a partially appearing primary; estimated primary obtained by 1D version [8] and by 2D version.

4. CONCLUSION

This paper proposes an adaptive filtering approach for multiple reflection cancellation in seismic data. The 2D anisotropic structure is taken into account and tackled using geometric multiscale representations and convex optimization. Although the proposed variational framework allows a wide range of sparse image representations to be used, directional dual-tree wavelets have demonstrated very good performance in our simulations and on real seismic images.

5. REFERENCES

[1] A. Guitton, "Multiple attenuation in complex geology with a pattern-based approach," *Geophysics*, vol. 70, no. 4, pp. V97–V107, 2005.

[2] S. Korman, D. Reichman, G. Tsur, and S. Avidan, "FasT-Match: Fast affine template matching," in *Proc. IEEE Conf. Comput. Vis. Pattern Recogn.*, Portland, OR, USA, Jun. 23-28, 2013, pp. 2331–2338.

[3] M. Liao, R. Yang, and Z. Zhang, "Robust and accurate visual echo cancelation in a full-duplex projector-camera system," *IEEE Trans. Pattern Anal. Mach. Intell.*, vol. 30, no. 10, pp. 1831–1840, Oct. 2008.

[4] M. Turka and C. Guillemot, "Image prediction: template matching vs. sparse approximation," in *Proc. Int. Conf. Image Process.*, Hong Kong, China, Sep. 26-29, 2010, pp. 789–792.

[5] L. Demanet and L. Ying, "Wave atoms and sparsity of oscillatory patterns," *Appl. Comp. Harm. Analysis*, vol. 23, no. 3, pp. 368–387, 2007.

[6] S. Ventosa, S. Le Roy, I. Huard, A. Pica, H. Rabeson, P. Ricarte, and L. Duval, "Adaptive multiple subtraction with wavelet-based complex unary Wiener filters," *Geophysics*, vol. 77, no. 6, pp. V183–V192, Nov.-Dec. 2012.

[7] S. Costagliola, P. Mazzucchelli, and N. Bienati, "Matched filtering with orthogonal constraints," in *Proc. EAGE Conf. Tech. Exhib.*, Copenhagen, Denmark, Jun. 4-7, 2012.

[8] M. Q. Pham, L. Duval, C. Chaux, and J.-C. Pesquet, "A primal-dual proximal algorithm for sparse template-based adaptive filtering: Application to seismic multiple removal," *IEEE Trans. Signal Process.*, vol. 62, no. 16, pp. 4256–4269, Aug. 2014.

[9] M. Q. Pham, C. Chaux, L. Duval, and J.-C. Pesquet, "A constrained-based optimization approach for seismic data recovery problems," in *Proc. Int. Conf. Acoust. Speech Signal Process.*, Florence, Italy, May 4-9, 2014, pp. 2377–2381.

[10] F. J. Herrmann and E. Verschuur, "Curvelet-domain multiple elimination with sparseness constraints," in *Annual International Meeting*, Denver, CO, USA, Oct. 10-15, 2004, pp. 1333–1336, Soc. Expl. Geophysicists.

[11] R. Neelamani, A. Baumstein, and W. S. Ross, "Adaptive subtraction using complex-valued curvelet transforms," *Geophysics*, vol. 75, no. 4, pp. V51–V60, 2010.

[12] J. Ma and G. Plonka, "The curvelet transform — a review of recent applications," *IEEE Signal Process. Mag.*, vol. 27, no. 2, pp. 118–133, Mar. 2010.

[13] D. Donno, "Improving multiple removal using least-squares dip filters and independent component analysis," *Geophysics*, vol. 76, no. 5, pp. V91–V104, 2011.

[14] Z. X. Li, W. K. Lu, and L. Liu, "Blind 2D convolved mixtures separation of primaries and multiples with non-Gaussian filters," in *Proc. EAGE Conf. Tech. Exhib.*, London, U. K., Jun. 10-13, 2013.

[15] L. Jacques, L. Duval, C. Chaux, and G. Peyré, "A panorama on multiscale geometric representations, intertwining spatial, directional and frequency selectivity," *Signal Process.*, vol. 91, no. 12, pp. 2699–2730, Dec. 2011.

[16] C. Chaux, L. Duval, and J.-C. Pesquet, "Image analysis using a dual-tree M-band wavelet transform," *IEEE Trans. Image Process.*, vol. 15, no. 8, pp. 2397–2412, Aug. 2006.

[17] C. Chaux, J.-C. Pesquet, and L. Duval, "Noise covariance properties in dual-tree wavelet decompositions," *IEEE Trans. Inf. Theory*, vol. 53, no. 12, pp. 4680–4700, Dec. 2007.

[18] C. Chaux, L. Duval, A. Benazza-Benyahia, and J.-C. Pesquet, "A nonlinear Stein based estimator for multichannel image denoising," *IEEE Trans. Signal Process.*, vol. 56, no. 8, pp. 3855–3870, Aug. 2008.

[19] N. Pustelnik, J.-C. Pesquet, and C. Chaux, "Relaxing tight frame condition in parallel proximal methods for signal restoration," *IEEE Trans. Signal Process.*, vol. 60, no. 2, pp. 968–973, Feb. 2012.

[20] N. Komodakis and J.-C. Pesquet, "Playing with duality: An overview of recent primal-dual approaches for solving large-scale optimization problems," *IEEE Signal Process. Mag.*, 2015.

[21] P. L. Combettes and J.-C. Pesquet, "Primal-dual splitting algorithm for solving inclusions with mixtures of composite, Lipschitzian, and parallel-sum type monotone operators," *Set-Valued Var. Anal.*, vol. 20, no. 2, pp. 307–330, Jun. 2012.

[22] J. J. Moreau, "Fonctions convexes duales et points proximaux dans un espace hilbertien," *C. r. Acad. Sci., Paris, Sér. A Math.*, vol. 255, pp. 2897–2899, 1962.

[23] P. L. Combettes and J.-C. Pesquet, "Proximal splitting methods in signal processing," in *Fixed-point algorithms for inverse problems in science and engineering*, H. H. Bauschke, R. Burachik, P. L. Combettes, V. Elser, D. R. Luke, and H. Wolkowicz, Eds., pp. 185–212. Springer Verlag, 2011.

[24] M. Q. Pham, " Seismic wave field restoration using sparse representations and quantitative analysis," *Ph.D. thesis*, Université Paris-Est, 2015.